Low-temperature, high-throughput spatial atomic layer deposition of NiOx nanocrystalline thin films from [Ni(ipki)2]

Samuel Porcar, Marcel Schmickler, Hayri Okcu, Jorit Obenlüneschloß, Stefano D'ercole, Laura Cervera- Gabalda, Itziar Galarreta-Rodriguez, Juan Rubio-Zuazo, Jaime Gonzalez Cuadra, Abderahim Lahlahi, et al.

Applied Surface Science Advances 29 (2025) 100836

Contents lists available at ScienceDirect

Applied Surface Science Advances

journal homepage: www.sciencedirect.com/journal/applied-surface-science-advances

Full Length Article

Low-temperature, high-throughput spatial atomic layer deposition of NiO_x nanocrystalline thin films from [Ni(^{i}pki)$_2$]

Samuel Porcar [a], Marcel Schmickler [b,c], Hayri Okcu [d,e], Jorit Obenlüneschloß [b], Stefano d'Ercole [d], Laura Cervera- Gabalda [f,g], Itziar Galarreta-Rodriguez [f,g], Juan Rubio-Zuazo [f,g], Jaime Gonzalez Cuadra [a], Abderahim Lahlahi [a], Diego Fraga [a], Camilo Sanchez-Velasquez [d], Daniel Bellet [d], Thomas Fix [h], Juan B. Carda [a], Anjana Devi [c,i,j], David Muñoz-Rojas [d,*]

[a] Universitat Jaume I de Castellón. Inorganic and Organic Chemistry Dept. Avguda Sos Baynat s/n 12071 Castellón, Spain
[b] Inorganic Materials Chemistry, Ruhr University Bochum, Bochum, Germany
[c] Leibnitz Institute for Solid State and Materials Research, 01069 Dresden, Germany
[d] Univ. Grenoble Alpes, CNRS, Grenoble INP, LMGP, 38000 Grenoble, France
[e] Univ. Grenoble Alpes, Univ. Savoie Mont Blanc, CNRS, Grenoble INP, CROMA, 38000 Grenoble, France
[f] Spanish CRG BM25-SpLine at The European Synchrotron, 71 Av. des Martyrs, 38000 Grenoble, France
[g] Instituto de Ciencia de Materiales de Madrid, CSIC, C/Sor Juana Inés de la Cruz 3, 28049 Madrid, Spain
[h] ICube laboratory, CNRS and Université de Strasbourg, 23 rue du Loess, 67037 Strasbourg, France
[i] Dresden University of Technology, 01062 Dresden, Germany
[j] Fraunhofer Institute for Microelectronic Circuits and Systems, 01159 Duisburg, Germany

ARTICLE INFO

Keywords:
NiO
Thin film
ALD
SALD
Transparent electrodes
Charge selective layers

ABSTRACT

Spatial atomic layer deposition (SALD) is a recent ALD variant enabling much faster deposition rates, even at atmospheric pressure, making it ideal for scalable, low-cost devices. NiO_x, a transparent p-type oxide, is widely used in emerging technologies like perovskite solar cells. However, no suitable SALD process for NiO thin films has been reported so far. In this work, we present the deposition of nanocrystalline NiO_x thin films via SALD using a recent Ni precursor not yet explored for the ALD of NiO, namely, bis(4-(isopropylamino)pent-3en-2-onato)nickel(II) or [Ni(^{i}pki)$_2$]. O_2 has been used as coreactant, with higher deposition rates being achieved if H_2O is added to the O_2 flow. A narrow ALD window has been obtained between 230 °C and 250 °C, where a GPC of 0.023 nm is observed. This corresponds to a deposition rate of 1.4 nm/min, which is 2 to 10 times faster than the rates reported for conventional ALD of NiO thin films. Remarkably, the growth onset of NiO_x starts around only 170 °C. The transmittance of the films reaches nearly 97 % in the visible for 55 nm thick films. Scanning electron microscopy (SEM) and transmission electron microscopy (TEM) studies revealed a high homogeneity of the films. X-ray diffraction (XRD), Raman spectroscopy and X-ray absorption spectroscopy (XAS) studies confirm the presence of a cubic NiO_x crystalline phase. Finally, NiO_x films have been deposited on Ag nanowire networks, demonstrating the possibility of depositing homogeneous and conformal coatings with this new process.

1. Introduction

Nickel (II) oxide (NiO) thin films have garnered significant attention due to their versatile properties and potential technological applications [1,2]. As a p-type semiconductor, NiO exhibits distinct electronic behaviour that includes high transmittance up to 97 %, good hole mobility (10^{-2} $cm^2 \cdot V^{-1} \cdot s^{-1}$), and a suitable work function for diverse optoelectronic devices. These properties make NiO appealing for a wide range of applications such as spanning radiation detectors, semiconducting devices, laser components, thermoelectric modules, and optoelectronic devices [3–6]. NiO crystallizes in a face-centered cubic structure and has a wide direct band gap that varies from 3.6 to 4 eV [7]. Given these specific properties, NiO has been extensively studied as hole transport layer in hybrid perovskite solar cells [8,9].

* Corresponding author.
E-mail address: david.munoz-rojas@grenoble-inp.fr (D. Muñoz-Rojas).

https://doi.org/10.1016/j.apsadv.2025.100836
Received 30 May 2025; Received in revised form 12 August 2025; Accepted 26 August 2025
Available online 3 September 2025

Different approaches have been developed to deposit NiO thin films, which have allowed to tailor thickness, morphology, composition, and crystalline structure. Between them, the most exploited deposition methods are spray pyrolysis [10–12], thermal decomposition [13], hydrothermal method [14,15], anodic arc plasma method [16], sol-gel [17,18], chemical bath deposition [19,20], sputtering [21,22] or atomic layer deposition (ALD) [23]. However, to the best of our knowledge, the majority of the mentioned methods require high temperatures (above 300 °C) to achieve high-quality NiO films, and in most cases, they are only viable for coating two-dimensional surfaces (except for ALD). This limitation restricts their application in advanced electronic devices that degrade at high temperatures like hybrid perovskite solar cells, or require more complex morphologies as certain chips and sensors [24].

Spatial atomic layer deposition (SALD) is a recent approach to ALD in which the precursors are separated in space rather than in time. This eliminates the need for a long purging step, while maintaining the key assets of ALD, that is, high conformality, thickness control below the nanometer scale and low-temperature deposition. As a result, SALD can reach higher deposition rates as compared to ALD, even when working at atmospheric pressure [25]. This vacuum-free and high-throughput process not only reduces complexity and operational cost but also makes SALD more compatible with industrial-scale production. Furthermore, SALD enables the fabrication of functional oxide films under realistic conditions and over large areas, providing a practical route toward the integration of these materials into commercial optoelectronic and energy devices [26]. In addition, as shown by the reports by Sekkat et al. on the deposition of Cu_2O thin films by SALD, by controlling the deposition conditions and the precursors used, SALD can yield oxide thin films with comparable and even superior properties than those obtained by PVD methods, such as PLD or sputtering, at higher temperatures [27,28]. Finally, we have shown that SALD can have a lower environmental impact than conventional ALD [29,30]. Despite the interest of developing a SALD process for the deposition of NiO thin films for hybrid perovskite solar cells and other devices, to date there are no reports in the literature. While B. Zhao et al. reported the deposition of NiO_x thin films using an SALD system, the growth takes place through chemical vapor deposition (CVD) rather than ALD [31].

In this work, we report the low-temperature, high-throughput SALD of NiO_x thin films. A recent Ni organometallic precursor bis(4-(isopropylamino)pent-3en-2-onato)nickel(II) or [Ni(^{i}pki)$_2$] was chosen as Ni precursor as it showed high volatility necessary for atmospheric pressure SALD and its mixed coordination of the Ni center with oxygen and nitrogen instills higher reactivity when compared to the β-diketonate type precursors often used for the ALD deposition of nickel materials [32]. To the best of our knowledge, this is the first time that this family of Ni compounds is evaluated for the (S)ALD deposition of NiO thin films. The growth process developed here achieves higher deposition rates than reported conventional ALD of NiO, without requiring vacuum systems, making it a more efficient and scalable route for industrial applications [33]. This work investigates the deposition of NiO thin films using SALD, exploring the process conditions, film characteristics, and growth behavior. The study examines the temperature dependence of the deposition, the structural and optical properties of the films, and their potential for conformal coating applications. A combination of scanning electron microscopy (SEM), transmission electron microscopy (TEM), X-ray diffraction (XRD), Raman spectroscopy and X-ray Absorption Spectroscopy (XAS) analyses was used to assess film homogeneity, crystallinity, and composition.

2. Experimental and methods

2.1. Film deposition

The NiO_x films were deposited using a homemade SALD system based on the close-proximity deposition technique, as described previously [34]. For the deposition, [Ni(^{i}pki)$_2$] and humid O_2 gas were used as Ni and O precursors, respectively. The films were grown on soda lime glass for microscope analysis. The substrates were previously immersed and sonicated in isopropanol and acetone baths for 5 min each. After the sonication, the glasses were dried under N_2 gas and used immediately. The flows used for each line are schematized in Fig. 1. The dilution line and bubbling line flows were 150 sccm respectively for the nickel precursor (injected via two precursor channels in the head). For the oxygen source, 450 sccm of O_2 were carried across the water bubbling line, without dilution (injected via four oxide gas channels in the head). The N_2 flow used for the barrier channels was 900 sccm injected via six channels. The nickel precursor bubbler was kept at 135 °C and the corresponding lines were heated to 175 °C. The water bubbler was kept at room temperature. The substrate temperatures were varied from 130 to 280 °C and the distance between the head and the substrate was kept at 100 µm. In the optimized procedure, the number of ALD cycles per sample was 2400 (600 SALD oscillations) to obtain a thickness of 55 nm with a substrate velocity of 51 mm/s. To facilitate the morphological and compositional study of the NiO_x by TEM, a selection of films was deposited on Ag nanowire (NW) networks as well. The networks were fabricated as detailed in previous works [34].

2.2. Deposition of Ag networks

Silver nanowires (AgNWs) suspended in isopropanol, with a silver concentration of 23.6 g/L, an average diameter of 70 nm, and a length of approximately 10 µm, were obtained from Protavic International. Before application, the nanowire dispersion was diluted according to previously reported protocols. Briefly, Corning glass substrates (25 × 25 mm^2) were subjected to ultrasonic cleaning for 15 min in both ethanol and deionized water, followed by nitrogen gas drying. A diluted AgNW solution (0.23 g/L in isopropanol) was spray-applied onto the glass surfaces using a standard airbrush system. The spraying process was carried out in a cross-hatched pattern, applying one droplet every six seconds under an air pressure of 1.4 bar. Substrates were maintained at 110 °C during deposition to enhance solvent evaporation and suppress the formation of coffee ring patterns.

Electrical resistance was continuously tracked during deposition using a two-probe multimeter setup. Silver paste was applied directly to the glass to form electrical contacts, allowing for in situ monitoring of the network's areal density. As a final step prior to the SALD process, all coated samples were thermally annealed at 200 °C for one hour.

2.3. Film characterization

The crystallinity of the films was assessed through Grazing Incidence X-ray Diffraction (GIXRD) using a D4 Endeavor diffractometer (Bruker-AXS) equipped with a Cu Kα radiation source. The data acquisition involved a step scan ranging from 20° to 80° (2θ), with increments of 0.05° and a dwell time of 5 s per step. Raman spectroscopy was performed using a WITec Apyron spectrometer with a 532 nm laser excitation source. Optical transmittance and band gap evaluations were conducted with a PerkinElmer Lambda 950 UV–Vis spectrophotometer, fitted with an integrating sphere, operating across the 250–900 nm range in 5 nm steps. The optical properties and thickness of the films were investigated by spectroscopic ellipsometry using a HORIBA Uvisel Lt M200 FGMS (210–880 nm) apparatus. Ellipsometric measurements were performed on samples grown on glass in the 1.4 eV - 5.9 eV spectral range.

Surface morphology and thickness were examined using a field emission scanning electron microscope (SEM-FEG, namelly, a Quanta 200 and GeminiSEM 300) and a JEOL JEM-1010 transmission electron microscope operating at 200 kV. The TEM setup included a JEOL EM-24830FLASH CMOS-based digital camera and an Oxford Aztec TEM Ultim Max EDS system, offering 127 eV resolution at the Mn K_α line and an 80 mm^2 window. A scanning Kelvin probe system (KP, KP

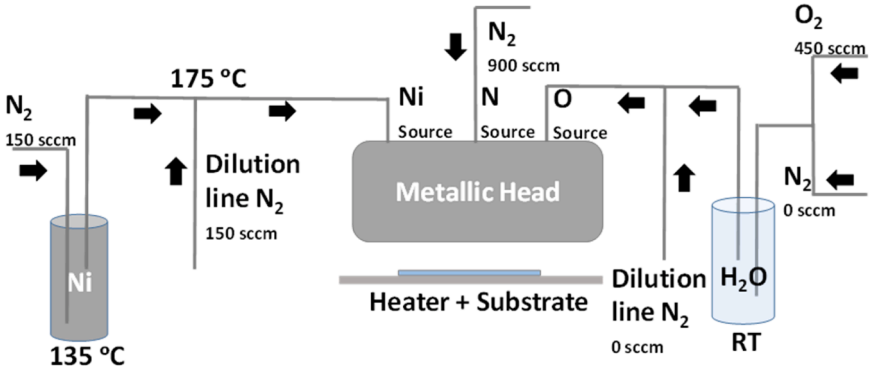

Fig. 1. Scheme of the open-air spatial atomic layer deposition (SALD) setup used for the deposition of NiO_x thin films.

Technology APS03) with a 2 mm diameter gold tip was used for work function (WF) determination and surface mapping in air. The WF of the tip was calibrated in an absolute way using an Ag sample measured by ambient-pressure photoemission spectroscopy (APS) in the same system.

Ni K-edge X-ray absorption spectroscopy (XAS) was carried out at beamline BM25 at the European Synchrotron Radiation Facility (ESRF) in Grenoble, France. Both X-ray absorption near edge structure (XANES) and extended X-ray absorption fine structure (EXAFS) spectra were acquired in fluorescence mode at ambient temperature. Calibration of the energy scale was done using a standard Ni metal foil. Data processing followed established protocols using the ATHENA software package [35, 36]. Atomic force microscopy (AFM) images were collected using a JEOL JSPM-5200 system in contact mode, scanning 2 μm × 2 μm areas.

3. Results and discussion

To determine the optimal deposition temperature, NiO_x films were deposited on glass substrates at different temperatures between 170 and 280 °C. Initial tests were performed using H_2O as oxygen precursor but no detectable film thickness was observed. O_2 was then tested and in this case deposition could be achieved with a low GPC. In order to enhance the deposition rate, humid O_2 was used, as described in the experimental part. It has been previously shown that adding H_2O to O_2 can have an impact on both rate and film properties during CVD processes [37]. Fig. 2a shows the growth per cycle (GPC) vs temperature for films obtained with 2400 ALD cycles. The maximum deposition rates were at 230 °C and 250 °C, which corresponds to the ALD window observed. The average GPC obtained in the window is 0.023 nm as can be seen in Fig. 2a. For lower and higher temperatures, a decrease in the GPC is observed, due to slow kinetics and precursor desorption, respectively [38]. While the obtained GPC using humid O_2 is still somewhat smaller than the reported GPC values for the ALD deposition of NiO_x, when converted to deposition rate, the films grow at a rate of 1.4 nm/min, which is 2 to 10 times faster than reported ALD values (see Table 1). For the samples deposited during 10 min, The low thickness of the layer prevented thickness measurements from being performed. It is also worth noting that the high deposition rate obtained for the process developed here is achieved without using ozone or plasma (as opposed to some of the reports listed in Table 1). Fig. 2b shows the layer growth as a function of time at a deposition temperature of 230 °C for different samples made for 10, 20, 30 and 40 min of deposition. Initially, a more pronounced growth is observed, attributed to the influence of the substrate, followed by a linear growth behavior, as expected.

The morphology of the film was evaluated by SEM. Figs. 3a and 3b show a cross-section and surface micrograph of a NiO_x film deposited on a glass substrate. As can be seen in Fig. 3b, the compact film presents a high uniformity. The topography of the films was studied by AFM. Fig. 3c shows a 3D image of the topography with the root-mean-squared roughness value, which is close to the roughness of the glass substrate (Figure S1a). To further assess the electronic uniformity of the surface, Kelvin Probe measurements were performed, (Supporting Figure 1b) showing a work function of 4.64 ± 0.01 eV with a standard deviation of only 0.02 eV across a 14 × 7 mm^2 area, confirming excellent homogeneity at the electronic level. Such low surface roughness can be beneficial for the use of these NiO_x films in (opto)electronic devices by generating better interfaces.

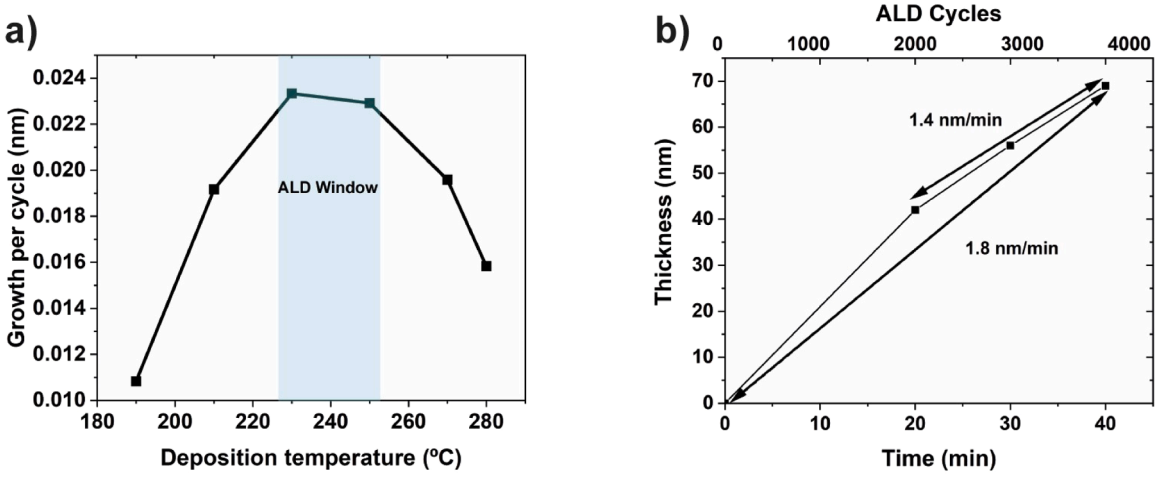

Fig. 2. a) Growth per cycle (GPC) for NiO_x films deposited at varying deposition temperatures for 2400 ALD cycles. b) Film thickness at different deposition times and number of ALD cycles with a substrate temperature of 230 °C.

Table 1
Comparison of the deposition parameters between this work and the bibliography.

Ni Precursor	Oxigen source	Temperature (°C)	Substrate	Crystallinity	Max. GPC (nm)	Growth rate (nm/min)	Ref.
$Ni(acac)_2$	O_3	250–310	Soda lime	Crystalline	0.077	0.77	[39]
$Ni(apo)_2$	O_3	190–310	Soda lime	Crystalline	0.062	0.67	[39]
$Ni(dmamp)_2$	H_2O	130	ZnO	Amorph	0.14	0.49	[40]
$Ni(thd)_2$	H_2O	205–275	SiO_2	Crystalline	0.04	0.11	[41]
$Ni(MeCp)_2$	O_2 plasma	250	Pt	Crystalline	0.058	0.2	[42]
$Ni(^ipki)_2$	**H_2O+O_2**	**190–280**	**Soda lime**	**Crystalline**	**0.023**	**1.4**	**This work**

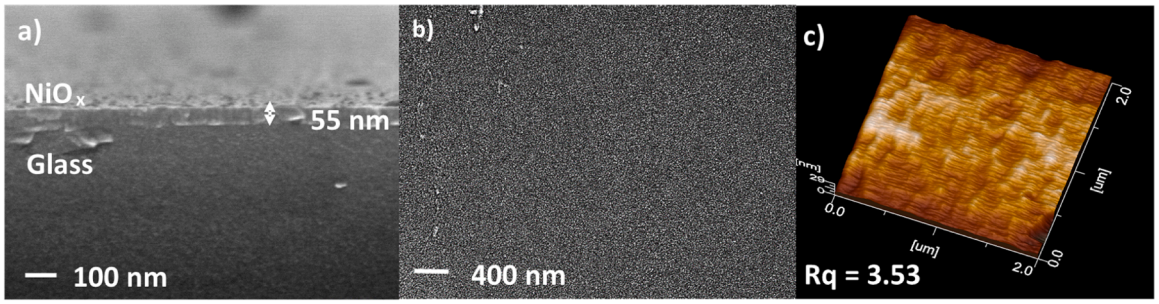

Fig. 3. Cross section (a) and surface (b) SEM micrographs of a NiO_x sample deposited at 230 °C. c) AFM 3D topography image.

Fig. 4a shows the XRD pattern of a 55 nm NiO_x film deposited at 230 °C measured by grazing incidence X-Ray diffraction (GIXRD) showing three main reflections indexed as the (111), (200), and (220) crystal planes of cubic NiO (reference diffraction pattern JCPDS: 01–089–3080). No peak corresponding to a secondary phase could be observed. To confirm the structure, a Raman spectroscopy study was also carried out. In this technique, the presence of local distortions or defects play an important role on the activation of some phonon modes and on their respective nature [43]. The Raman spectrum and its deconvolution is shown in Fig. 4b In it, different bands related with the NiO_x structure were assigned according to the literature [44–46]. The peaks at 372 cm^{-1}, 529 cm^{-1} and 650 cm^{-1} are associated with the TO, LO_1 and LO_2 modes. Several additional phonon modes were as well detected, namely, a TO+one-magnon peak at 469 cm^{-1}, a 2TO mode at 819 cm^{-1} and the LO+TO and 2LO peaks respectively at 958 cm^{-1} and 1083 cm^{-1}. It is also observed that the size of the LO peak is larger than that of the 2LO, which is associated with a small particle size according to the literature (**see Figure S2**) [47].

The transmittance results of a set of samples deposited with 2400 ALD cycles at different temperatures are shown in Fig. 5a in the wavelength range between 350 and 800 nm. The average transmittance in the visible part of the spectra for the samples was near 97 % making it a good candidate for optoelectronic applications, namely, in transparent electrodes or for transparent oxide junctions [48]. The decrease in the transmittance with the temperature can be attributed to the increase in the thickness of the NiO_x films due to the increase in the GPC. It can be observed that at 130 °C there is no growth. While film growth was possible at 170 °C (where a decrease in the transmittance is observed), the growth rate was too low to be practical. Consequently, the GPC was calculated starting from 190 °C. As observed in Fig. 5a, the absorption increases until 230 °C, coinciding with the highest GPC obtained. After it, a small decrease in absorption is observed for the samples deposited at 270 °C and 280 °C, in agreement with the obtained ALD window. The inset shows a picture of a bare glass substrate (on the left) and a coated (one on the right) placed on the LMGP logo, demonstrating the high transparency of the film (the top part of the slides comes with a colored white and blue layer for the purpose of labelling).

In addition to UV–Vis absorption spectroscopy, spectroscopic ellipsometry was used to determine the optical constants. Fig. 5b shows the n and k values for a 88 nm thick film deposited a 230 °C. Considering an indirect transition, as expected for NiO, the extracted bandgap from the ellipsometry data was 3.53±0.05 eV, which is in agreement with literature values [49]. From this data, an energy diagram could be plotted (shown in **Figure S3).**

The local electronic structure of the NiO_x thin films was investigated using XANES and EXAFS at the Ni K-edge. Fig. 6a shows the normalized XANES spectra for the NiO_x thin films deposited at different temperatures. As can be observed, the spectra exhibit four prominent characteristics. First, a low energy pre-edge peak is observed for all the samples at 8335 eV, correlated with the 1s → 3d electronic quadrupole transition

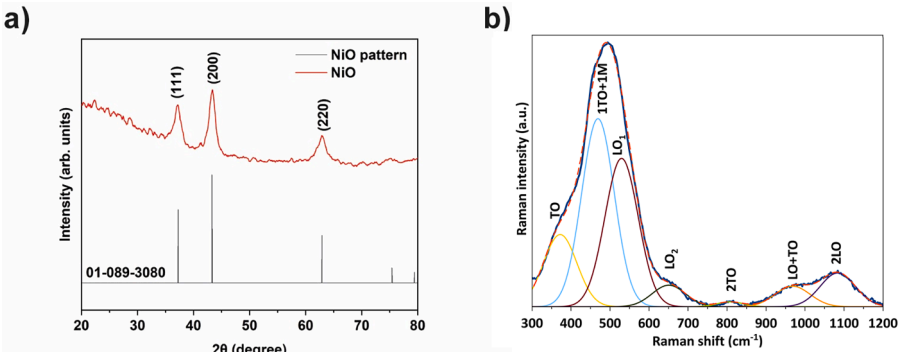

Fig. 4. a) GIXRD and b) corresponding Raman spectrum for a 55 nm thick NiO_x thin film deposited at 230 °C.

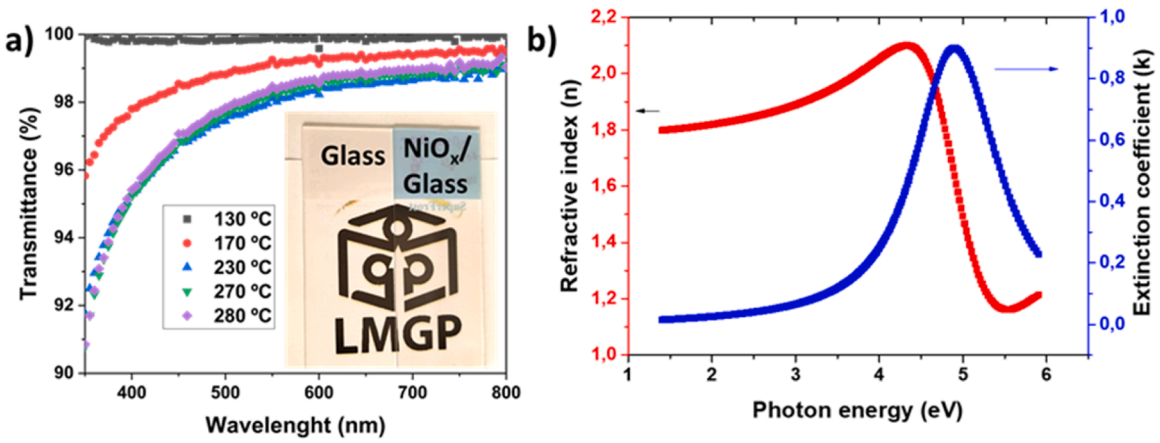

Fig. 5. a) Transmittance (without the glass) for samples deposited at different temperatures for 2400 ALD cycles. The thickness of the films deposited at 130, 170, 230, 270 and 280 °C were 0, ≈12, 55, 47 and 38 nm respectively. The inset in a) shows a photo of the sample compared with a bare glass substrate. b) n,k values vs. photon energy obtained from spectroscopic ellipsometry for a 88 nm thick NiO_x sample deposited at 230 °C on glass.

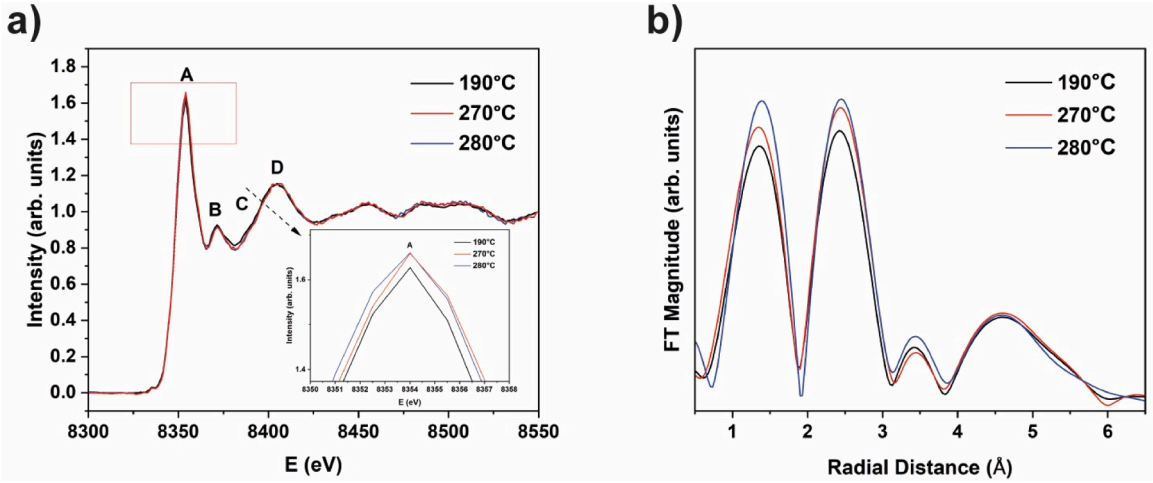

Fig. 6. Ni K-edge XAS spectra for the NiO_x thin films deposited at 190, 270 and 280 °C. (a) Near-edge X-ray absorption region (XANES), and (b) magnitude of the Fourier-transformed EXAFS (Extended X-ray Absorption Fine Structure) spectra.

of Ni^{2+} in the octahedral geometry (Oh) [50,51]. A well-defined and intense resonance feature, labeled as peak A, is observed next. This peak, commonly known as the white line in XANES spectra, arises from electronic transitions between the 1s core level and unoccupied 4p states. Following this, subtle structures denoted as B and C can be observed within the multiple scattering region between 8360 and 8380 eV. Lastly, there is a broad D peak, which exhibits single-scattering-like behavior and is positioned at a higher energy level compared to the initial EXAFS oscillation (around 8400 eV). This specific feature is indicative of an octahedral geometry within a cubic lattice, and it aligns consistently with previously reported data for NiO_x [52]. These four features are intrinsic from crystalline NiO indicating the successful formation of crystalline NiO_x thin films even for a deposition temperature as low as 190 °C.

Subtle differences can be seen as a function of the deposition temperature. In the XANES region, a slight decrease (0.03) in the intensity of the A peak in the sample deposited at 190 °C is observed in Fig. 6a, an indication of the presence of lower coordination states around Ni atoms in comparison to the other samples. The intensity of the white line increases indeed with deposition temperature, as previously reported in the literature [53]. Therefore, these results suggest that decreasing the temperature of the process leads to a reduced coordination number around Ni atoms in NiO_x thin films. Such an effect on the deposition temperature is also observed in the EXAFS region. The EXAFS spectra provide insight into the radial distribution of neighboring atoms around Ni atoms. Representing the Fourier transform's magnitude visually illustrates the scattering distances between the absorbing atom and its closest neighbors. Fig. 6b displays the k^3-weighted Fourier-transformed EXAFS spectra at the Ni K-edge for the thin films. The initial peak, located at approximately 1.35 Å, corresponds to the radial distribution of oxygen atoms bonded to nickel (indicative of Ni–O interactions). The subsequent peak, appearing near 2.43 Å, is associated with scattering contributions from neighboring nickel atoms, reflecting Ni–Ni coordination involving twelve surrounding Ni atoms [54]. The peak's intensity offers information about the level of order of both bonds. A subtle change in peak intensity is observed among each film, suggesting a minor influence of deposition temperature on the atomic arrangements of Ni-O and Ni-Ni bonds [55,56]. Intensity increases as the deposition temperature of the films is increased. This fact coincides with that previously mentioned in the XANES section, which indicates that a higher crystallinity is obtained as the preparation temperature is increased.

To explore the conformality of our SALD process, NiO_x films were also grown on AgNW networks at 230 °C [34]. Fig. 7 shows SEM and TEM results of the coated networks. In Fig. 7a, uniform and conformal NiO_x films with a thickness of approximately 35 nm over the Ag NWs can be observed in the SEM image (especially for the wires in focus at the

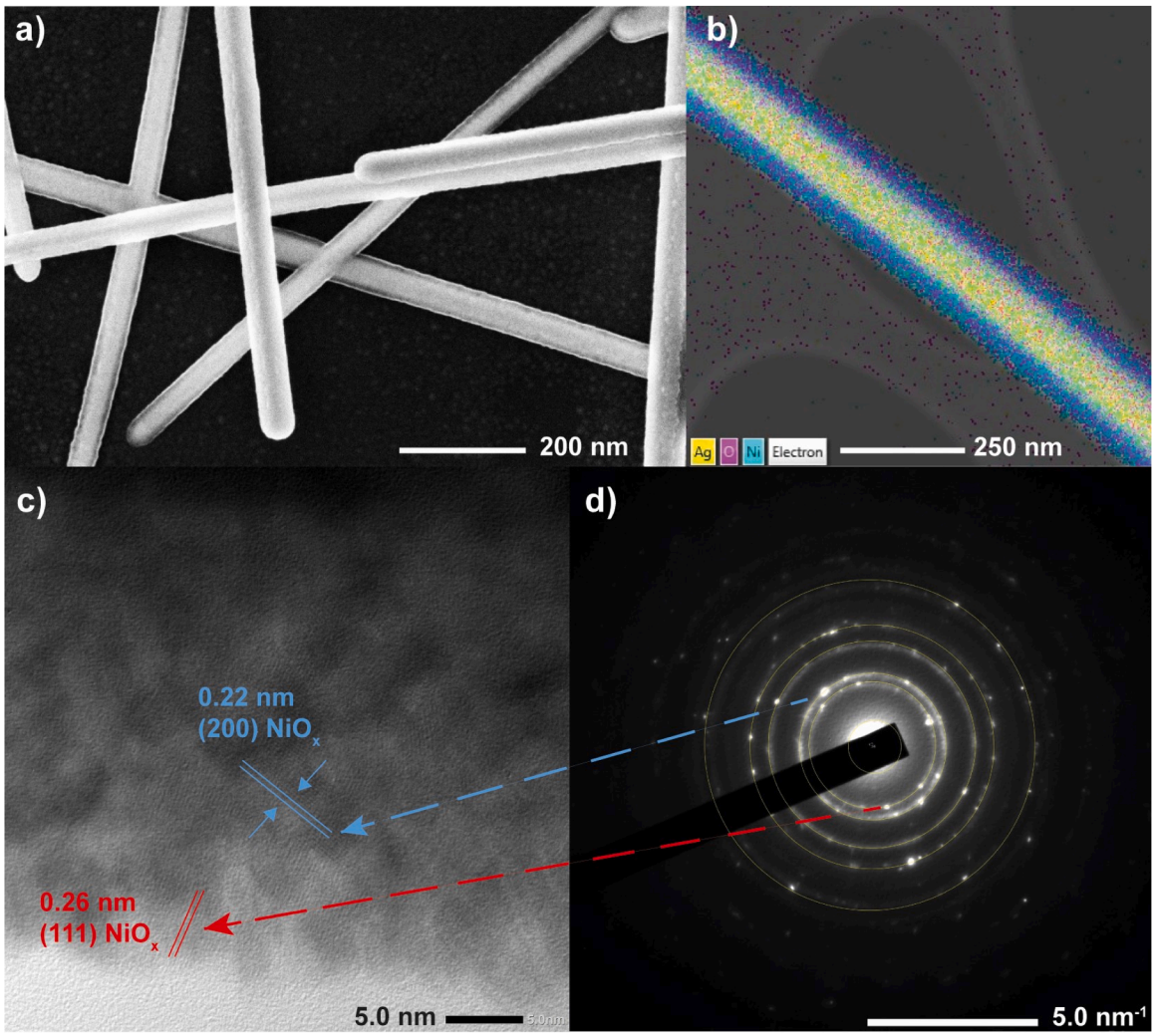

Fig. 7. a) SEM and b) TEM micrographs of Ag NWs coated with NiO_x thin films deposited at 230 °C. c), d) TEM image with a SAED pattern of a 20 nm thick NiO_x thin film deposited on a silver nanowire at 230 °C.

bottom of the image). Fig. 7b shows a TEM micrograph that includes a compositional mapping obtained by EDS. It can be observed how the yellow points (Ag) only appear in the core of the nanowire. Conversely, the Ni signal has a constant presence on and around the Ag signal, indicating that the Ag NWs is conformally coated with a NiO_x film (full spectrum of elements available in Supporting information, **Figure S4**). Fig. 7c shows HRTEM results and it can be observed that the film is composed of various particles of approximately 5 nm showing crystalline planes with spacing that is in agreement with the NiO_x cubic phase (see SAED pattern in Fig. 7d), in agreement with the GIXRD results.

4. Conclusions

We reported a new SALD deposition process for the deposition of NiO_x films using $[Ni(^{i}pki)_2]$ as Ni precursor, being the first time this precursor is used for the (S)ALD deposition of NiO thin films. NiO_x films could be synthesized at relatively low temperatures near 190 °C and without the need of hazardous oxygen precursors like ozone or plasma requiring complex reactor setups. A combination of O_2 and water was used to improve the GPC of the deposition process. The process showed an ALD widow between 230 °C and 250 °C, where a GPC of 0.023 nm is obtained (corresponding to a deposition rate of 2.1 nm/min). The obtained deposition rate is up to 2 to 10 times faster than for previously reported NiO ALD processes. The combination of high deposition rate, operation under atmospheric pressure and in an open setup makes this new process very appealing for industrial implementation. XRD, Raman spectroscopy and XAS results confirmed the deposition of cubic NiO_x films. The thin films are smooth, closed and highly transparent (nearly 97% in the visible for 55 nm thick films deposited at 230 °C), as desired for an ALD process. The excellent conformality of the process was demonstrated by coating AgNW networks. This work highlights the potential of SALD as a scalable, vacuum-free, and high-throughput method for the synthesis of high-quality NiO_x films, offering a promising pathway for their integration into industrial optoelectronic and energy-related technologies.

CRediT authorship contribution statement

Samuel Porcar: Writing – original draft, Investigation, Formal analysis. **Marcel Schmickler:** Writing – review & editing, Investigation. **Hayri Okcu:** Writing – review & editing, Investigation. **Jorit Obenlüneschloß:** Writing – review & editing, Formal analysis. **Stefano d'Ercole:** Writing – review & editing, Investigation. **Laura Cervera-Gabalda:** Writing – review & editing, Formal analysis. **Itziar Galarreta-Rodriguez:** Writing – review & editing, Data curation. **Juan Rubio-Zuazo:** Writing – review & editing, Formal analysis. **Jaime Gonzalez Cuadra:** Writing – review & editing, Investigation. **Abderahim Lahlahi:** Writing – review & editing, Investigation. **Diego Fraga:** Supervision. **Camilo Sanchez-Velasquez:** Writing – review & editing, Investigation. **Daniel Bellet:** Writing – review & editing, Supervision.

Thomas Fix: Investigation. **Juan B. Carda:** Writing – review & editing, Supervision, Funding acquisition. **Anjana Devi:** Writing – review & editing, Supervision, Conceptualization. **David Muñoz-Rojas:** Writing – review & editing, Supervision, Funding acquisition, Conceptualization, Formal analysis, Methodology, Project administration.

Declaration of competing interest

The authors declare the following financial interests/personal relationships which may be considered as potential competing interests: Samuel Porcar Garcia reports financial support was provided by University Jaume I. If there are other authors, they declare that they have no known competing financial interests or personal relationships that could have appeared to influence the work reported in this paper.

Acknowledgements

The authors would like to express their gratitude for the financial support provided by several research initiatives: the FOTOCER project (PID2020–116149GB-I00), funded by MCIN/AEI/10.13039/501100011033; the CLUSCERM project (TED2021–130963B-C22), supported by MCIN/AEI/10.13039/501100011033 and the European Union's NextGenerationEU/PRTR initiative; and the CLUSKER project (INNEST/2024/420), funded by the Valencian Institute of Business Competitiveness (IVACE). Additional support was received from the, jointly funded by ANR (project number 21-CE08–0047) and DFG (project number 490773082). The work has also benefited from funding under the Investissement d'Avenir (PIA) program – LabEx MINOS. Furthermore, the authors acknowledge support through the post-doctoral fellowship CIAPOS/2023/425 and the predoctoral fellowship CIACIF/2022/277, both co-financed by the Valencian regional government and the European Social Fund. Authors also want to thank the "Cátedra de Innovación Cerámica 'Ciutat de Vila-real' de l'Universitat Jaume I" for the financial support. We also acknowledge the Spanish Ministerio de Ciencia, Innovación y Universidades and Consejo Superior de Investigaciones Científicas for financial support and for provision of synchrotron radiation facilities through the projects 2010 6 0E 013, 2021 60 E 030 and CEX2024-001445-S. Finally, We thank Carmen Jiménez for technical support and discussions.

Supplementary materials

Supplementary material associated with this article can be found, in the online version, at doi:10.1016/j.apsadv.2025.100836.

Data availability

Data will be made available on request.

References

[1] A. Yakubu, S. Sahabi, S.G. Danjumma, Y. Abubakar, S. Suleiman, Nickel oxide (NiO) devices and applications: a review, Int. J. Eng. Res. Technol. (IJERT) 8 (04) (2019). April-ISSN: 2278-0181.

[2] M. Napari, T.N. Huq, R.L.Z. Hoye, J.L. MacManus-Driscoll, Nickel oxide thin films grown by chemical deposition techniques: potential and challenges in next-generation rigid and flexible device applications, InfoMat 3 (5) (2021) 536–576, https://doi.org/10.1002/inf2.12146, may.

[3] R. Paulose, R. Mohan, V. Parihar, Nanostructured nickel oxide and its electrochemical behaviour—a brief review, in: Nano-Structures and Nano-Objects, 11, Elsevier B.V., Jul. 01, 2017, pp. 102–111, https://doi.org/10.1016/j.nanoso.2017.07.003.

[4] S.A. Makhlouf, K.M.S. Khalil, Variable range hopping conduction in NiO/Al2O3 nanocomposites, Int. J. Nanosci. 4 (2) (2005), https://doi.org/10.1142/S0219581X05003024.

[5] H. Sato, T. Minami, S. Takata, and T. Yamada, "Transparent conducting p-type NiO thin films prepared by magnetron sputtering," 1993.

[6] M. Kitao, K. Izawa, K. Urabe, Komatsu T, S. Kuwano, S. Yamada, Preparation and electrochromic properties of RF-sputtered NiOx films prepared in Ar/O2/H2 atmosphere, Jpn. J. Appl. Phys 33 (6656) (1994), https://doi.org/10.1143/JJAP.33.6656.

[7] M. Jlassi, I. Sta, M. Hajji, H. Ezzaouia, Synthesis and characterization of nickel oxide thin films deposited on glass substrates using spray pyrolysis, Appl. Surf. Sci. 308 (Jul. 2014) 199–205, https://doi.org/10.1016/j.apsusc.2014.04.134.

[8] W. Chen, et al., Understanding the doping effect on NiO: toward high-performance inverted perovskite solar cells, Adv. Energy Mater. 8 (19) (Jul. 2018), https://doi.org/10.1002/aenm.201703519.

[9] B. Zhang, et al., NiO/perovskite heterojunction contact engineering for highly efficient and stable perovskite solar cells, Adv. Sci. 7 (11) (Jun. 2020), https://doi.org/10.1002/advs.201903044.

[10] E.P. Etape, O.E. Agbor, B.V. Namondo, Z. Benmaamar, J. Foba-Tendo, J.N. Lambi, Synthesis, characterization, and effects of morphology on the magnetic application base properties of pure nickel oxide (NiO) and cobalt-doped nickel oxide/nickel hydroxide nanocomposites, Adv. Nanopart. 12 (03) (2023) 106–122, https://doi.org/10.4236/anp.2023.123009.

[11] Z. El Khalidi, S. Fadili, B. Hartiti, A. Lfakir, P. Thevenin, M. Siadat, Behavior of NiO thin films sprayed at different annealing time, Opt. Quantum Electron. 48 (9) (Sep. 2016), https://doi.org/10.1007/s11082-016-0694-8.

[12] H.S. Rasheed, H.I. Abdulgafour, F.M. Hassan, A.A. Najim, Synthesis, characterization, and gas-sensing performance of macroporous Zn-doped NiO thin films for ammonia gas detection, J. Mater. Sci. 33 (23) (Aug. 2022) 18187–18198, https://doi.org/10.1007/s10854-022-08675-y.

[13] S. Legmairi, et al., Biofabrication of NiO and NiO-decorated Fe nanocomposite efficiency for removal of methylene blue from aqueous solution, Biomass Convers. Biorefin. (2023), https://doi.org/10.1007/s13399-023-03912-8.

[14] S. Ashok C, A. Vazhayil, J. Thomas, N. Thomas, Enhanced electrochemical performance of facilely synthesized cobalt doped cubic NiO nanoflakes for supercapacitor application, J. Energy Storage 55 (Nov. 2022), https://doi.org/10.1016/j.est.2022.105498.

[15] R. Kaliyaperumal, S. Paramasivam, S. Boonyuen, V. PoovanBull, Fabrication of hydrothermal-assisted NiO/ZnO nanohybrid and their antimicrobial activity, Mater. Sci. 46 (147) (2023), https://doi.org/10.1007/s12034-023-02994-4.

[16] A. Pol, S. Sapakal, A. Khan, A.V. Kadam, Synthesis of NiO thin film on 304-grade stainless steel substrate for oxygen evolution reaction, Surf. Interfaces 37 (Apr. 2023), https://doi.org/10.1016/j.surfin.2023.102706.

[17] Y.M.S. Jamil, M.A.H. Awad, H.M.A. Al-Maydama, Y. EL-Ghoul, A.N. Al-Hakimi, Synthesis and study of enhanced electrochemical properties of NiO nanoparticles deposited on TiO_2 nanotubes, Appl. Organomet. Chem. 36 (9) (Sep. 2022), https://doi.org/10.1002/aoc.6795.

[18] K. Haunsbhavi, D. Alagarasan, N.J. Shivaramu, H.M. Mahesh, P. Murahari, B. Angadi, Nanostructured NiO thin film for ammonia sensing at elevated temperatures, J. Electron. Mater. 51 (11) (Nov. 2022) 6356–6368, https://doi.org/10.1007/s11664-022-09859-2.

[19] J. Baek, Y. Kim, K.H. Baik, S. Jang, H_2S sensing characteristics of NiO nanopetal film, ECS J. Solid State Sci. Technol. 12 (8) (Aug. 2023) 085002, https://doi.org/10.1149/2162-8777/ace8bc.

[20] C. Aiempanakit, M. Aiempanakit, W. Thongjoon, S. Pudwat, K. Aiempanakit, Characterization and electrochromic properties of multi-morphology NiO films prepared by CBD and DC techniques, Opt. (Stuttg.) 287 (Sep. 2023), https://doi.org/10.1016/j.ijleo.2023.171131.

[21] X. Gao, X. Meng, Effect of reactive pressure on direct current-sputtered NiO films with improved p-type conduction ability, Phys. B Condens. Matter 650 (Feb. 2023), https://doi.org/10.1016/j.physb.2022.414540.

[22] A.R.M. Alghamdi, M. Yanagida, Y. Shirai, G.G. Andersson, K. Miyano, Surface passivation of sputtered NiO_x using a SAM interface layer to enhance the performance of perovskite solar cells, ACS Omega 7 (14) (Apr. 2022) 12147–12157, https://doi.org/10.1021/acsomega.2c00509.

[23] S. Seo, I. Park, M. Kim, S. Lee, C. Bae, H. Jung, N.-G. Park, J. Young Kim, H. Shin, An ultra-thin, un-doped NiO hole transporting layer of highly efficient (16.4%) organic–inorganic hybrid perovskite solar cells, Nanoscale 8 (22) (2016) 11403–11412, https://doi.org/10.1039/C6NR01601D.

[24] J.H. Park, J. Seo, S. Park, S.S. Shin, Y.C. Kim, N.J. Jeon, H.-W. Shin, T.K. Ahn, J. H. Noh, S.C. Yoon, C.S. Hwang, S.I. Seok, Efficient $CH_3NH_3PbI_3$ perovskite solar cells employing nanostructured p-type NiO electrode formed by a pulsed laser deposition, Adv. Mater. 27 (27) (2015) 4013–4019, https://doi.org/10.1002/adma.201500523, jul.

[25] L. Johnston, J. Obenlüneschloß, M. Niazi, M. Weber, C. Lausecker, L. Rapenne, H. Roussel, C. Sanchez-Velazquez, D. Bellet, A. Devi, D. Muñoz-Rojas *a, Assessing the potential of non-pyrophoric $Zn(DMP)_2$ for the fast deposition of ZnO functional coatings by spatial atomic layer deposition, RSC Appl. Interfaces 1 (6) (2024) 1371–1381, https://doi.org/10.1039/D4LF00160E.

[26] D. Muñoz-Rojas, J. MacManus-Driscoll, Spatial atmospheric atomic layer deposition: a new laboratory and industrial tool for low-cost photovoltaics, Mater. Horiz. 1 (3) (2014) 314–320, https://doi.org/10.1039/C3MH00136A.

[27] A. Sekkat, O. Liedke, V.H. Nguyen, M. Butterling, F. Baiutti, J.S. Veru, M. Weber, L. Rapenne, D. Bellet, G. Chichignoud, A. Kaminski-Cachopo, E. Hirschmann, A. Wagner, D. Muñoz-Rojas, Chemical deposition of Cu_2O films with ultra-low resistivity: correlation with the defect landscape, Nat. Commun. 13 (1) (2022) 5322, https://doi.org/10.1038/s41467-022-32943-4, sep.

[28] A. Sekkat, V.H. Nguyen, C.A. Masse de La Huerta, et al., Open-air printing of Cu_2O thin films with high hole mobility for semitransparent solar harvesters, Commun. Mater. 2 (2021) 78, https://doi.org/10.1038/s43246-021-00181-8.

[29] M. Weber, N. Boysen, O. Graniel, A. Sekkat, C. Dussarrat, P. Wiff, A. Devi, D. Muñoz-Rojas, Assessing the environmental impact of atomic layer deposition

(ALD) processes and pathways to lower it, ACS Mater. Au 3 (4) (2023) 274–298, https://doi.org/10.1021/acsmaterialsau.3c00002, jul.
[30] M.F.K. Niazi, D. Muñoz-Rojas, D. Evrard, M. Weber, Comparative study of the environmental impact of depositing Al_2O_3 by atomic layer deposition and spatial atomic layer deposition, ACS Sustain. Chem. Eng. 11 (41) (2023) 15072–15082, https://doi.org/10.1021/acssuschemeng.3c04135, oct.
[31] B. Zhao, L.C. Lee, L. Yang, et al., In situ atmospheric deposition of ultrasmooth nickel oxide for efficient perovskite solar cells, ACS Appl. Mater. Interfaces 10 (2018) 41849–41854.
[32] D. Zywitzki, et al., Tuning coordination geometry of nickel ketoiminates and its influence on thermal characteristics for chemical vapor deposition of nanostructured NiO electrocatalysts, Inorg. Chem. 59 (14) (Jul. 2020) 10059–10070, https://doi.org/10.1021/acs.inorgchem.0c01204.
[33] R.L.Z. Hoye, et al., Spatial atomic layer deposition for energy and electronic devices, PRX Energy 4 (1) (Feb. 2025), https://doi.org/10.1103/prxenergy.4.017002.
[34] V.H. Nguyen, et al., Deposition of ZnO based thin films by atmospheric pressure spatial atomic layer deposition for application in solar cells, J. Renew. Sustain. Energy 9 (2) (Mar. 2017), https://doi.org/10.1063/1.4979822.
[35] B. Ravel, M. Newville, ATHENA, ARTEMIS, HEPHAESTUS: data analysis for X-ray absorption spectroscopy using IFEFFIT, J. Synchrotron Radiat. (Jul. 2005) 537–541, https://doi.org/10.1107/S0909049505012719.
[36] N. Fairley, et al., Systematic and collaborative approach to problem solving using X-ray photoelectron spectroscopy, Appl. Surf. Sci. Adv. 5 (Sep. 2021) 100112, https://doi.org/10.1016/j.apsadv.2021.100112.
[37] Y. Wu, et al., Atomic layer deposition of In_2O_3:H from InCp and H_2O/O_2: microstructure and isotope labeling studies, ACS Appl. Mater. Interfaces 9 (1) (Jan. 2017) 592–601, https://doi.org/10.1021/acsami.6b13560.
[38] R.L. Puurunen, Growth per cycle in atomic layer deposition: a theoretical model, Chem. Vap. Depos. 9 (5) (2003) 249–257, https://doi.org/10.1002/cvde.200306265, oct.
[39] M. Utriainen, M. Kröger-Laukkanen, L. Niinistö, Studies of NiO thin film formation by atomic layer epitaxy, Mater. Sci. Eng. B 54 (1–2) (Jun. 1998) 98–103, https://doi.org/10.1016/S0921-5107(98)00135-4.
[40] J.H. Yang, S.Y. Lee, W.S. Song, Y.S. Shin, C.-Y. Park, H.-J. Kim, W. Cho, K.-S. An, Field emission properties of ZnO nanorods coated with NiO film, J. Vac. Sci. Technol. B Microelectron. Nanom. Struct. Process. Meas. Phenom. 26 (3) (May 2008) 1021–1024, https://doi.org/10.1116/1.2919156.
[41] E. Lindahl, M. Ottosson, J.O. Carlsson, Atomic layer deposition of NiO by the Ni $(thd)_2/H_2O$ precursor combination, Chem. Vap. Depos. 15 (7–9) (Sep. 2009) 186–191, https://doi.org/10.1002/cvde.200906762.
[42] S.J. Song, et al., Substrate dependent growth behaviors of plasma-enhanced atomic layer deposited nickel oxide films for resistive switching application, Chem. Mater. 24 (24) (Dec. 2012) 4675–4685, https://doi.org/10.1021/cm302182s.
[43] N. Bala, H.K. Singh, S. Verma, S. Rath, Magnetic-order induced effects in nanocrystalline NiO probed by Raman spectroscopy, Phys. Rev. B 102 (2) (Jul. 2020), https://doi.org/10.1103/PhysRevB.102.024423.
[44] N. Mironova-Ulmane, A. Kuzmin, I. Sildos, L. Puust, J. Grabis, Magnon and phonon excitations in nanosized NiO, Latv. J. Phys. Tech. Sci. 56 (2) (Apr. 2019) 61–72, https://doi.org/10.2478/lpts-2019-0014.
[45] M. Terlemezoglu, O. Surucu, M. Isik, N.M. Gasanly, M. Parlak, Temperature-dependent optical characteristics of sputtered NiO thin films, Appl. Phys. Mater. Sci. Process. 128 (1) (Jan. 2022), https://doi.org/10.1007/s00339-021-05197-y.
[46] S. Suman, A. Behra, P. Swaminathan, Oxygen-modulated photoresponse in nickel oxide thin films for wide band gap photodetector application, Discov. Appl. Sci. 7 (1) (Jan. 2025) 84, https://doi.org/10.1007/s42452-025-06485-5.
[47] W.J. Duan, S.H. Lu, Z.L. Wu, Y.S. Wang, Size effects on properties of NiO nanoparticles grown in alkalisalts, J. Phys. Chem. C 116 (49) (2012) 26043–26051, https://doi.org/10.1021/jp308073c, dic.
[48] P. Barquinha, R. Martins, L. Pereira, E. Fortunato, Transparent Oxide Electronics: From Materials to Devices, Wiley, 2012. ISBN: 978-1-119-96774-3.
[49] K.J. Rietwyk, et al., Universal work function of metal oxides exposed to air, Adv. Mater. Interfaces 6 (12) (Jun. 2019), https://doi.org/10.1002/admi.201802058.
[50] J.P. Hill, C.-C. Kao, and D.F. Mcmorrow, "K-edge resonant x-ray magnetic scattering from a transition-metal oxide: niO," 1997.
[51] F. Sajid, N. Jabeen, L.U. Khan, M. Sohail, A. Rehman, Z. Akhter, Local atomic structure order and electrochemical properties of NiO based nano-catalysts for ethanol sensing at room temperature, J. Phys. Chem. Solids 175 (Apr. 2023), https://doi.org/10.1016/j.jpcs.2022.111201.
[52] Q. Hu, et al., Direct confirmation of confinement effects by NiO confined in helical SnO_2 nanocoils and its application in sensors, J. Mater. Chem. Mater. 10 (6) (Feb. 2022) 2786–2794, https://doi.org/10.1039/d1ta08630h.
[53] S.P. Thompson, Structural signatures of medium-range order in annealed laboratory silicates, Astron. Astrophys. 484 (1) (Jun. 2008) 251–265, https://doi.org/10.1051/0004-6361:20078675.
[54] Y.R. Denny, et al., Electronic, electrical and optical properties of undoped and Na-doped NiO thin films, Thin Solid Films (Sep. 2015) 255–260, https://doi.org/10.1016/j.tsf.2015.04.043.
[55] A. Trivedi, R.J. Choudhary, A. Das, S.K. Rai, M.K. Tiwari, A.K. Sinha, Surface-interface investigations of an ultrathin pulsed laser deposited NiO/ZnO bilayer structure, Surf. Interface Anal. 52 (9) (Sep. 2020) 533–540, https://doi.org/10.1002/sia.6774.
[56] T. Kim, J. Lee, G. Park, H. Lee, Synthesis of nonstoichiometric NiO nanocatalysts and growth of bamboo-like carbon nanotubes, Int. J. Appl. Ceram. Technol. 18 (5) (Sep. 2021) 1527–1532, https://doi.org/10.1111/ijac.13807.